

## RESEARCH ACTIVITIES II

### Department of Molecular Structure

## II-A Picosecond Transient Infrared Studies on Excited States of Donor-Acceptor Systems

Molecules having an electron donor and acceptor group at both ends of a conjugated  $\pi$ -electron system sometimes show characteristic photophysical behavior: dual fluorescence, for example. 4-(Dimethylamino)benzonitrile (DMABN) has attracted much attention as a prototype of such compounds. The photophysics of these compounds are thought to be closely related to excited state molecular structures. We have already published static/transient infrared studies on DMABN and isotopomers in the ground state and in the charge-transfer excited state [*J. Phys. Chem. A* **104**, 4182 (2000); *Chem. Phys.* **260**, 193 (2000); *J. Phys. Chem. A* **105**, 4182 (2001)]. As an extension of that, we have studied molecular structures of excited states of DMABN and analogues by means of picosecond infrared spectroscopy.

### II-A-1 Picosecond Infrared Spectrum of 4-(Pyrrol-1-yl)benzonitrile: Structure of the Excited Charge-Transfer States of Donor-Acceptor Systems

OKAMOTO, Hiromi<sup>1,2</sup>; KINOSHITA, Mariko<sup>2</sup>  
(<sup>1</sup>IMS; <sup>2</sup>Univ. Tokyo)

[*J. Phys. Chem. A* submitted]

Picosecond transient infrared spectrum of the excited charge-transfer (CT) state of 4-(pyrrol-1-yl)benzonitrile (PBN) has been recorded in the frequency range of 1700–920  $\text{cm}^{-1}$ . The CT state of PBN gives several quite strong infrared bands. The band at 1219  $\text{cm}^{-1}$  shifts toward high-frequency side with increasing delay time between pump and probe pulses. This frequency shift is attributed to vibrational relaxation. Some of the transient bands (1429, ~1290, 1219, and 964  $\text{cm}^{-1}$ ) are very close in frequencies to those observed for the benzonitrile moiety of the excited CT state of 4-(dimethylamino)benzonitrile (DMABN). This finding implies that benzonitrile groups of PBN and DMABN are decoupled from the electron donating (pyrrole or dimethylamino) groups, and it can be explained by the twisted intramolecular charge transfer model. To make this point clear, however, further discussion is necessary on the band assignments and on correlation between structure and spectral pattern.

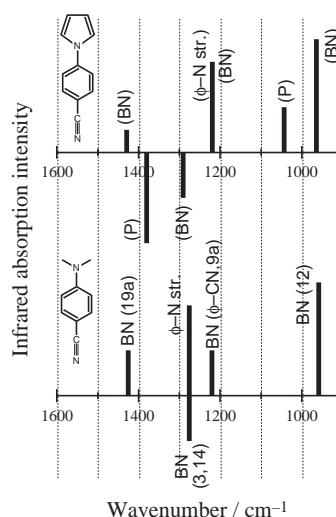


**Figure 1.** Transient infrared spectral patterns for the excited CT states of PBN (top) and DMABN (bottom). Tentative band assignments are given in parentheses for PBN. BN, mode of benzonitrile moiety; P, mode of pyrrole moiety.

### II-A-2 Picosecond Infrared Spectra and Structure of Locally Excited and Charge Transfer Excited States of Isotope Labeled 4-(Dimethylamino)benzonitriles

OKAMOTO, Hiromi<sup>1,2</sup>; KINOSHITA, Mariko<sup>2</sup>;  
KOHTANI, Shigeru<sup>3</sup>; NAKAGAKI, Ryoichi<sup>3</sup>;  
ZACHARIASSE, Klaas A.<sup>4</sup>

(<sup>1</sup>IMS; <sup>2</sup>Univ. Tokyo; <sup>3</sup>Kanazawa Univ.; <sup>4</sup>Max-Planck Inst.)

[*Bull. Chem. Soc. Jpn.* submitted]

Infrared spectra of the ground, charge transfer (CT), and locally excited (LE) states of isotope-labeled 4-(dimethylamino)benzonitriles (DMABNs) in the region between 1700 and 900  $\text{cm}^{-1}$  are reported. The isotopomers measured are normal DMABN,  $\text{NC-C}_6\text{H}_4\text{-}^{15}\text{NMe}_2$  (dimethylamino nitrogen labeled DMABN), and  $\text{NC-C}_6\text{H}_2\text{D}_2\text{-NMe}_2$  (3,5-dideuterated DMABN). Infrared spectrum of the excited CT state of DMABN-

$d_2$  is consistent with the previous band assignments for normal DMABN and DMABNs isotopically labeled on dimethylamino group. For the LE state of normal DMABN, three bands are observed at 1481, 1415, and  $1399\text{ cm}^{-1}$ . This is in contrast with a previously reported transient infrared spectrum, where positions of bands due to the transient do not shift from the ground state ones. The band at *ca.*  $1481\text{ cm}^{-1}$  is observed for normal and  $^{15}\text{N}$  labeled DMABN, but not for DMABN- $d_2$ . Except for this point, the band positions are almost identical for the three isotope-labeled species. The vibrational transitions observed at *ca.* 1415 and  $1398\text{ cm}^{-1}$  are hence attributed to modes with atomic displacements localized on methyl groups and/or the part of the benzonitrile moiety adjacent to the cyano group or the cyano group itself. Quantum chemical calculations of the vibrational spectra for the CT and LE states of DMABN at present do not correctly reproduce the experimental spectra, which means that more accurate calculations are needed for a reliable analysis of these spectra.

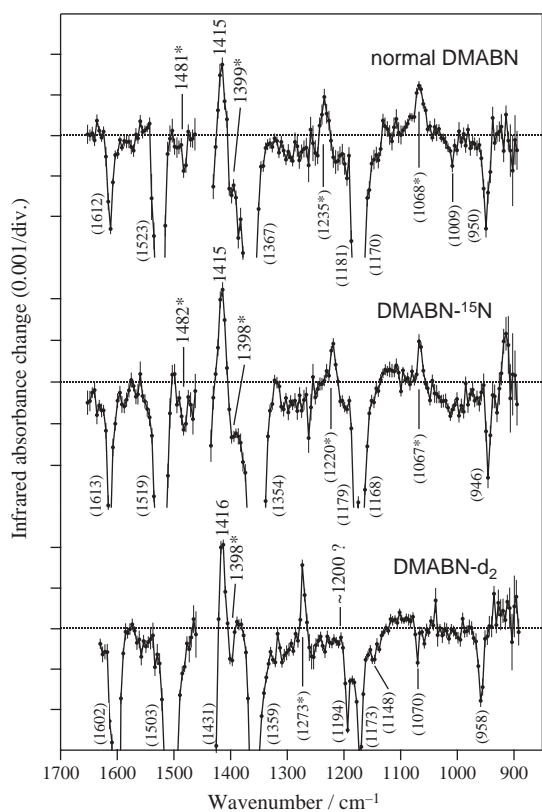


**Figure 1.** Transient infrared spectra of DMABN and the two isotope-labeled derivatives DMABN- $d_2$  and DMABN- $^{15}\text{N}$  in cyclohexane solution at room temperature at 4 ps after excitation. Bleached bands arising from the ground state are indicated in parentheses. Negative bands due to non-totally symmetric vibrational modes (for both the ground and the excited states) are marked with asterisks.

## II-B Laser Cooling and Trapping of Metastable Helium Atoms

In the past two decades, extensive developments have occurred in the laser cooling and trapping of neutral atoms, with many workers reporting the application of these techniques to such diverse atomic species as alkali atoms, alkali earth atoms, and rare gas atoms. Among these, the helium atom is unique on account of its small mass, simple energy level structure, and easy availability in two isotopic forms ( $^3\text{He}$  and  $^4\text{He}$ ) of differing quantum statistics. For this reason, we have been studying the laser cooling and trapping of helium atoms.

### II-B-1 Magneto-Optical Trap of Metastable Helium Atoms with Doughnut Laser Beams: Computer Simulations

MORITA, Norio

When we intend to confine metastable helium atoms in high density in a magneto-optical trap (MOT), it is always a critical problem that the collisional ionization loss of the atoms is tremendously large under the irradiation of trapping laser light near-resonant with the cooling transition ( $2s^3S_1 \rightarrow 2p^3P_2$ ). One of the possible methods that can let us avoid this problem may be to use laser beams with doughnut intensity profiles, because a MOT composed of such laser beams has almost negligible laser intensity around the MOT center. However, such a MOT has never been investigated so far and it is not trivial whether this type of MOT can efficiently confine the atoms. Therefore, with a computer simulation we have examined the availability of this MOT. First let us consider a one-dimensional MOT composed of doughnut laser beams: in this case, an atom lying at the center of the beam cross section and moving parallel to the beam axis receives no force

from the beam, and so this atom can be neither decelerated nor trapped by the beam. This means that it is necessary to stop up the "hole" of the MOT by, for example, additional laser beams. Taking this into consideration, we can find that the simplest and most symmetric three-dimensional MOT that has no such "holes" may be a MOT with a dodecahedral beam configuration, which consists of eight doughnut beams coming from apexes of a dodecahedron to its center. Note that this configuration can easily be realized by a simple modification of a usual tetrahedral configuration. We have numerically simulated the atomic motion in this type of MOT, which is composed of eight laser beams with ( $n = 0, l = 1$ ) Laguerre-Gaussian intensity profiles (the peak intensity is  $20 \text{ mW/cm}^2$  and the radius of the peak ring is 3 mm). Consequently, we have found that any atom can be confined within a radius of 0.1 mm, in which only  $< 0.5\%$  of the atoms are excited into the upper state of the cooling transition by the lasers. This means that the atomic density in the MOT can be increased by a factor of more than five in comparison with an ordinary MOT in the full saturation condition. An experiment to prove this result is now in progress.

## II-C Spectroscopic Studies on Atoms and Ions in Liquid Helium

Atoms and ions in liquid helium are known to reside in bubble-like cavities due to the Pauli repulsive force between electrons. Physical properties of these exotic surroundings are determined by the potential energy of the impurity- $\text{He}_n$  system, the surface tension energy of the liquid helium, and the pressure-volume work. Spectroscopic studies of such impurity atoms and ions in liquid helium are expected not only to give information on the structure and dynamics of the bubbles but also to contribute to the study on the property of superfluid liquid helium.

### II-C-1 Investigation on the Difference between Spectra of Ca Atoms in Liquid $^3\text{He}$ and $^4\text{He}$

MORIWAKI, Yoshiki<sup>1</sup>; MORITA, Norio  
(<sup>1</sup>Toyama Univ.)

Spectra of impurity atoms in liquid helium often explicitly reflect physical properties of the liquid. In this meaning, it may especially be interesting to investigate the difference between spectra of impurity atoms in liquid  $^3\text{He}$  and  $^4\text{He}$ , because even at a temperature as high as 1.4 K these liquids have much different physical properties; for example, the density is  $1.62 \times 10^{22}$  and  $2.19 \times 10^{22} \text{ cm}^{-3}$  for  $^3\text{He}$  and  $^4\text{He}$ , respectively, and the

surface tension is 0.116 and 0.336 dyn/cm for  $^3\text{He}$  and  $^4\text{He}$ , respectively. These differing properties are mainly caused by differences in the mass and quantum statistics between each species of He. In this work we have experimentally obtained spectra of Ca atoms in liquid  $^3\text{He}$  and  $^4\text{He}$  at 1.4 K and have investigated their differences. The experimental excitation spectra of the  $4s^2 \ ^1S_0 \rightarrow 4s4p \ ^1P_1$  and  $4s4p \ ^3P_{0,1,2} \rightarrow 4s5s \ ^3S_1$  transitions are shown in Figures 1 (a) and (b), respectively. For each transition, as seen in these figures, the spectrum for liquid  $^3\text{He}$  is narrow compared with the one for liquid  $^4\text{He}$ , and the blue-shift of the former spectrum is smaller than the latter. This fact can qualitatively be explained with differences in the

number density and surface tension of the liquid; namely, in liquid  $^3\text{He}$ , the size of a bubble formed around an impurity Ca atom is larger because of the smaller number density and surface tension of liquid  $^3\text{He}$ , and this causes the Ca-He interaction the weaker. To confirm this, we have theoretically calculated these spectra, assuming a model Hamiltonian describing the Ca atom, bubble and their interactions for each liquid He. This Hamiltonian has almost the same form as assumed in our previous work on  $\text{Yb}^+$  in liquid He. The spectra thus calculated are shown in Figures 1 (c) and (d), corresponding to Figures 1 (a) and (b), respectively. Comparing Figures 1 (a) and (b) with Figures 1 (c) and (d), respectively, we can see that the calculated results considerably well reproduce both widths and shifts of the experimental spectra. This fact strongly suggests that the differences observed in the experimental spectra are mainly caused by the differences in the physical properties of liquid  $^3\text{He}$  and  $^4\text{He}$ .

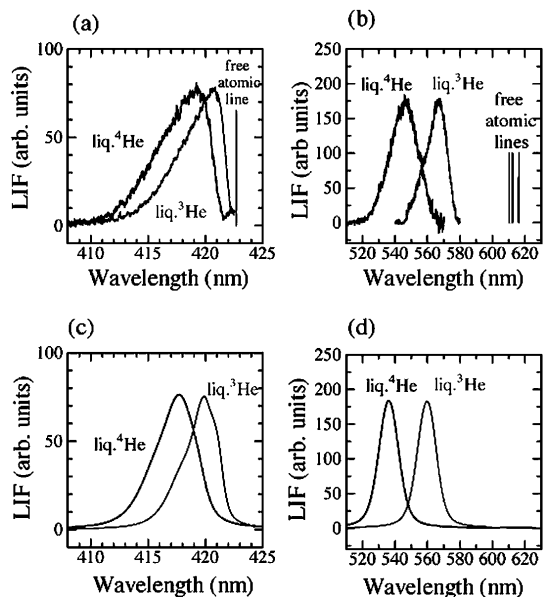


**Figure 1.** Excitation spectra of Ca atoms in liquid  $^3\text{He}$  (gray curves) and  $^4\text{He}$  (black curves): (a) and (b) show the experimental spectra of the  $4s^2\ ^1S_0 \rightarrow 4s4p\ ^1P_1$  and  $4s4p\ ^3P_{0,1,2} \rightarrow 4s5s\ ^3S_1$  transitions, respectively, and the theoretical spectra of those transitions are shown in (c) and (d), respectively. In (a) and (b), each transition wavelength of the free atom is also shown with a solid vertical line.

## II-D Laser Spectroscopic Studies on Collisional Fine Structure Changing Transitions of Atoms and Ions

The fine structure changing transition in atoms and ions due to collisions with other particles is one of the important processes for the energy transportation in interstellar gases as well as in the atmosphere. However, unexpectedly, the number of studies so far devoted to the measurement of the cross section for this process is not so large. For this reason, we have been studying this process with laser spectroscopic methods, mainly focusing on alkali-earth ions, which have simpler energy level structures and so allow us to analyze experimental results more easily.

### II-D-1 Laser Spectroscopic Measurements of Fine Structure Changing Cross Sections of $\text{Ba}^+$ Ions in Collisions with He Atoms

MORIWAKI, Yoshiki<sup>1</sup>; MATSUO, Yukari<sup>2</sup>;  
MORITA, Norio  
(<sup>1</sup>Toyama Univ.; <sup>2</sup>RIKEN)

We have measured the cross section of the fine structure changing  $6p\ ^2P_{3/2} \rightarrow 6p\ ^2P_{1/2}$  transition of the  $\text{Ba}^+$  ion in collisions with He atoms at a room temperature. Like our similar work on  $\text{Ca}^+$  and  $\text{Sr}^+$ ,  $\text{Ba}^+$  ions have been produced by laser ablation of a piece of  $\text{BaTiO}_3$  placed in a vacuum chamber. The chamber is filled with He gas, and the ions produced are immediately cooled to a room temperature through collisions with the He atoms. Exciting the ions into the  $6p\ ^2P_{3/2}$  level and detecting the laser-induced fluorescence from  $6p\ ^2P_{3/2}$  and the sensitized

fluorescence from  $6p\ ^2P_{1/2}$  we have successfully obtained cross sections of the collision-induced  $6p\ ^2P_{3/2} \rightarrow 6p\ ^2P_{1/2}$  transition and of the collisional quenching in the  $6p\ ^2P_{1/2}$  level:  $\sigma(6p\ ^2P_{3/2} \rightarrow 6p\ ^2P_{1/2}) = (2.9 \pm 0.4) \times 10^{-4}\ \text{\AA}^2$  and  $\sigma(6p\ ^2P_{1/2} \rightarrow \text{all states}) = (4.2 \pm 7.9) \times 10^{-2}\ \text{\AA}^2$ . Figure 1 shows the cross sections for the  $np\ ^2P_{3/2} \rightarrow np\ ^2P_{1/2}$  transitions of various alkali metal atoms as well as alkali earth ions in the logarithmic scale as a function of their fine structure splittings. As seen in Figure 1, the cross sections for the alkali atoms are almost on a straight line; those for the alkali earth ions are also roughly on a straight line, but its slope is much different from the one for the alkali atoms. These exponential decreases common to both the ions and atoms can be explained by the Landau-Zener theory, as described in the previous work. On the other hand, the differing slopes of the decreases may be due to a difference between the interactions for ion-He and atom-He pairs; namely, the interaction in an ion-He pair is mainly the

monopole-induced-dipole interaction, which is stronger than for an atom-He pair. This fact may result in that, assuming the same fine structure splitting, the cross section for an alkali earth ion is much larger than for an alkali atom, as seen in Figure 1.

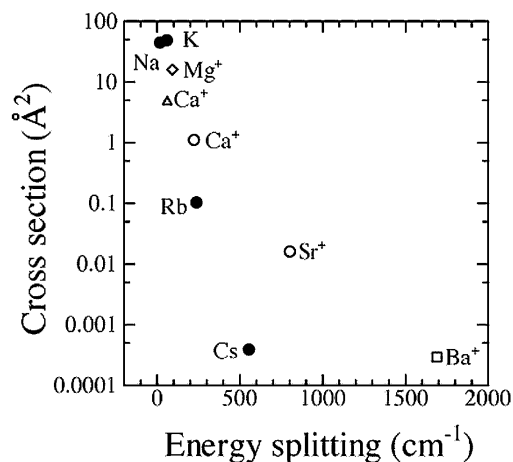


**Figure 1.** Fine structure changing cross sections so far measured for various alkali atoms and alkali earth ions in collisions with He atoms, as a function of their fine structure splittings; ● shows the one for the  $np\ ^2P_{3/2} \rightarrow np\ ^2P_{1/2}$  transition of each alkali atom ( $n = 3, 4, 5$  and  $6$ , and the collision temperature  $T = 397, 368, 340$  and  $311$  K for Na, K, Rb and Cs, respectively) (by Krause), ◇  $Mg^+ 3p\ ^2P_{3/2} \rightarrow 3p\ ^2P_{1/2}$  at 1600 K (by Brust *et al.*), △  $Ca^+ 3d\ ^2D_{5/2} \rightarrow 3d\ ^2D_{3/2}$  at 10000 K (by Knoop *et al.*), ○  $Ca^+ 4p\ ^2P_{3/2} \rightarrow 4p\ ^2P_{1/2}$  and  $Sr^+ 5p\ ^2P_{3/2} \rightarrow 5p\ ^2P_{1/2}$  at 298 K (by Moriwaki *et al.*) and □ the present data.

## II-D-2 Measurements of Fine Structure Changing Cross Sections of $Ca^+$ , $Sr^+$ and $Ba^+$ Ions due to Collisions with $H_2$ and $D_2$ Molecules

MORIWAKI, Yoshiki<sup>1</sup>; MATSUO, Yukari<sup>2</sup>;  
MORITA, Norio  
(<sup>1</sup>Toyama Univ.; <sup>2</sup>RIKEN)

Because of the vibrational and rotational degrees of freedom in molecules, fine structure changing transitions of ions due to collisions with molecules may show unique properties different from the ones in collisions with spherical atoms like He. For this reason, we have measured cross sections for such transitions of  $Ca^+$ ,  $Sr^+$  and  $Ba^+$  ions in collisions with  $H_2$  and  $D_2$  molecules. The experimental procedure is almost the same as in the previous ion-He collision studies, except for filling the vacuum chamber with  $H_2$  or  $D_2$  gas instead of He. The cross sections obtained are summarized in Table 1. For the  $np\ ^2P_{3/2} \rightarrow np\ ^2P_{1/2}$  transitions, as seen in Table 1, there are no drastic differences in the cross sections among each ion. This is completely different from the behavior seen in collisions with He. On the other hand, it is quite interesting that the ratio between the cross sections for the collisions with  $H_2$  and  $D_2$  decreases with the increase of the fine structure splitting, which is 222, 802 and  $1690\text{ cm}^{-1}$  for  $Ca^+$ ,  $Sr^+$  and  $Ba^+$ , respectively. Considering this fact as well as the sizes of the splittings, we can find that not vibrational transitions but

rotational transitions of the molecules resonantly contribute to the collisional fine structure changing transitions of the ions. To confirm this, we have theoretically calculated the cross section ratios, based on a semi-classical theory (Anderson-Tsao-Curnutte theory) taking into consideration the degree of resonance between fine structure splittings of the ions and rotational transitions of the molecules. As seen in Table 1, the experimental ratios are well reproduced by our theoretical calculation.

**Table 1.** Fine structure changing cross sections of  $Ca^+$ ,  $Sr^+$  and  $Ba^+$  due to collisions with  $H_2$  and  $D_2$ .

Ion	Transition	Cross Sections ( $\text{\AA}^2$ )		$\sigma(D_2)/\sigma(H_2)$	
		$\sigma(H_2)$	$\sigma(D_2)$	exp.	calc.
$Ca^+$	$4p\ ^2P_{3/2} \rightarrow 4p\ ^2P_{1/2}$	$13.2 \pm 0.6$	$18.7 \pm 0.8$	1.4	1.6
$Ca^+$	$4p\ ^2P_{1/2} \rightarrow 4p\ ^2P_{3/2}$	$20.5 \pm 0.9$	$27.1 \pm 1.3$	1.3	
$Sr^+$	$5p\ ^2P_{3/2} \rightarrow 5p\ ^2P_{1/2}$	$22.7 \pm 0.4$	$18.0 \pm 0.4$	0.82	0.7
$Ba^+$	$6p\ ^2P_{3/2} \rightarrow 6p\ ^2P_{1/2}$	$11.5 \pm 0.1$	$3.9 \pm 0.2$	0.33	0.3

## II-E Endohedral Metallofullerenes: New Fullerene Molecules with Novel Properties

Encapsulation of one or more metal atoms inside hollow fullerene cages (endohedral metallofullerenes) has long attracted special attention because it could lead to new spherical molecules with novel properties unexpected for empty fullerenes. Great efforts have been made for the production and characterization of endohedral metallofullerenes. Up to now it has been demonstrated that group 2 and 3 metals and most lanthanide metals can be trapped inside the higher fullerenes to form soluble and relatively stable endohedral metallofullerenes. Because of the difficulty in producing pure samples in large quantities, the experimental characterization of endohedral metallofullerenes has been hindered. Recent important progress is marked by the successful isolation and purification of metallofullerenes in macroscopic quantities. This has made it possible to investigate the interesting electronic properties and chemical reactivities.

### II-E-1 Structural Determination of the La@C<sub>82</sub> Isomer

AKASAKA, Takeshi<sup>1</sup>; WAKAHARA, Takatsugu<sup>2</sup>; NAGASE, Shigeru<sup>3</sup>; KOBAYASHI, Kaoru<sup>3</sup>; WÄLCHLI, Markus<sup>4</sup>; YAMAMOTO, Kazunori<sup>5</sup>; KONDO, Masahiro<sup>2</sup>; SHIRAKURA, Shingo<sup>2</sup>; MAEDA, Yutaka<sup>2</sup>; KATO, Tatsuhisa; KAKO, Masahiro<sup>6</sup>; NAKADAIRA, Yasuhiro<sup>6</sup>; GAO, Xiang<sup>7</sup>; VAN CAEMELBECKE, Eric<sup>7</sup>; KADISH, Karl M.<sup>7</sup>

(<sup>1</sup>IMS and Niigata Univ.; <sup>2</sup>Niigata Univ.; <sup>3</sup>Tokyo Metropolitan Univ.; <sup>4</sup>Bruker Japan; <sup>5</sup>PRN; <sup>6</sup>Univ. Electro-Commun.; <sup>7</sup>Univ. Houston)

[*J. Phys. Chem. B* **105**, 2971 (2001)]

A stable diamagnetic monoanion of the La@C<sub>82</sub> isomer was electrochemically prepared and isolated in order to disclose its cage symmetry. By measuring the <sup>13</sup>C NMR spectrum of the anion, it was determined for the first time that the isomer has C<sub>s</sub> symmetry, as was also confirmed by density functional calculations.

### II-E-2 Structure of La<sub>2</sub>@C<sub>80</sub> Studied by La K-Edge XAFS

KUBOZONO, Yoshihiro<sup>1</sup>; TAKABAYASHI, Yasuhiro<sup>1</sup>; KASHINO, Setsuo<sup>1</sup>; KONDO, Masahiro<sup>2</sup>; WAKAHARA, Takatsugu<sup>2</sup>; AKASAKA, Takeshi<sup>3</sup>; KOBAYASHI, Kaoru<sup>4</sup>; NAGASE, Shigeru<sup>4</sup>; EMURA, Shuichi<sup>5</sup>; YAMAMOTO, Kazunori<sup>6</sup>

(<sup>1</sup>Okayama Univ.; <sup>2</sup>Niigata Univ.; <sup>3</sup>IMS and Niigata Univ.; <sup>4</sup>Tokyo Metropolitan Univ.; <sup>5</sup>Osaka Univ.; <sup>6</sup>PRN)

[*Chem. Phys. Lett.* **335**, 163 (2001)]

The structure of La<sub>2</sub>@C<sub>80</sub> is studied by La K-edge XAFS from 40 to 295 K. The distances between the La atom and the first nearest C atoms, and between the La atom and the second nearest C atoms have been determined to be 2.42(1) Å at 40 K and 2.44(2) Å at 295 K, and 2.97(2) Å at 40 K and 2.98(3) Å at 295 K, respectively. The La–La distance has also been determined to be 3.90(1) Å at 40 K and 3.88(2) Å at 295 K. The dynamical behavior of two La atoms in the C<sub>80</sub>

cage is also studied based on the temperature dependence of the mean-square displacement of La–C.

## II-F Electron Transfer Regulation in a Tetraheme-Cytochrome, Cytochrome $c_3$

Cytochrome  $c_3$  is an electron transport protein found in several species of sulfate-reducing bacteria. This protein is a small (M.W.  $\approx$  14,000) soluble protein and possesses four  $c$ -type hemes per molecule. Cytochrome  $c_3$  has unique properties. It shows very low oxidation-reduction (redox) potentials (typically,  $-240 \sim -357$  mV vs. NHE), and the solid film of the reduced cytochrome  $c_3$  was shown highly electro-conductive. The macroscopic and microscopic redox potentials were determined for a variety of sulfate-reducing bacteria. The major aims of this project is to elucidate the mechanism of the regulation of the electron transfer in cytochrome  $c_3$  on the basis of tertiary structure. For this purpose, we have established a new and efficient expression system of  $c$ -type multiheme cytochromes for the first time. By the use of this expression system, structural determination of the fully reduced cytochrome  $c_3$  from *Desulfovibrio vulgaris* Miyazaki F by NMR and analysis of oxidation-reduction properties using amino acid replacement are going on.

### II-F-1 A Simple, Rapid, and Highly Efficient Gene Expression System for Multiheme-Cytochromes $c$

OZAWA, Kiyoshi<sup>2</sup>; YASUKAWA, Fumiko<sup>2</sup>;  
FUJIWARA, Yumiko<sup>2</sup>; AKUTSU, Hideo<sup>1,2</sup>  
(<sup>1</sup>IMS and Osaka Univ.; <sup>2</sup>Yokohama Natl. Univ.)

[*Biosci., Biotechnol., Biochem.* **65**, 185 (2001)]

It is important to establish a simple and highly efficient gene expression system of  $c$ -type cytochromes for the wide variety of studies such as physicochemical analyses, bioelectronics, environmental chemistry, and biotechnology. Especially, a large-scale preparation of a multiheme cytochrome  $c$  and its related mutants such as the amino acid replacements are very difficult. The difficulty in preparing  $c$ -type cytochromes is due to the complexity of the protein maturation, which needs various specific enzymes such as signal sequence peptidase and heme lyase. For this reason the heterologous expression of a  $c$ -type cytochrome is a special challenge. Here, we have exploited the potential of *S. oneidensis* by using the pUC-type universal vectors for *E. coli* in the transformation and have established a much more efficient gene expression system. The genes of tetraheme cytochrome  $c_3$  and hexadecaheme high molecular weight cytochrome  $c$  from *Desulfovibrio vulgaris* were overexpressed in *Shewanella oneidensis* MR-1 using pUC-type vectors to yield the periplasmic holoforms. Covalent multiheme attachments were successfully performed in *S. oneidensis*. Furthermore, it was shown that *S. oneidensis* could be directly transformed by a pUC-type vector of *E. coli* through electroporation. Transcription of the heterologous gene in *S. oneidensis* could be controlled by a *lac* promoter from *E. coli*. These results indicate that *S. oneidensis* can be used as an overexpression system for  $c$ -type multiheme-cytochrome genes using the well established genetic techniques in *E. coli*. In conclusion, a rapid, simple, and highly efficient gene expression system of  $c$ -type multiheme cytochromes in a heterologous host has been established. This system would open a new horizon in various studies such as electron transfer mechanism, bioelectronics, and environmental chemistry.

### II-F-2 Structure Determination of the Fully Reduced Cytochrome $c_3$ From *D. vulgaris* Miyazaki F

HARADA, Erisa<sup>1,2,3</sup>; FUKUOKA, Yuki<sup>3</sup>;  
OHMURA, Tomoaki<sup>4</sup>; FUKUNISHI, Arima<sup>3</sup>;  
KAWAI, Gota<sup>5</sup>; FUJIWARA, Toshimichi<sup>2</sup>;  
AKUTSU, Hideo<sup>1,2</sup>

(<sup>1</sup>IMS; <sup>2</sup>Osaka Univ.; <sup>3</sup>Yokohama Natl. Univ.;  
<sup>4</sup>Mitsubishi Heavy Industries; <sup>5</sup>Chiba Inst. Tech.)

Heteronuclear NMR spectroscopy was used for calculation of the solution structural ferrocycytochrome  $c_3$  from *Desulfovibrio vulgaris* Miyazaki F (*DvMF*). From 3D TOCSY-HSQC and NOESY-HSQC experiments, all <sup>15</sup>N and <sup>1</sup>H backbone signals except N-terminus and Pro residues were assigned. To complete side chain assignment, 2D DQF-COSY, TOCSY, and NOESY experiments were performed. A total number of 633 proton signals were assigned, which correspond to 97% of the total number of expected signals. At first, NOEs from NH signals were collected using 3D NOESY-HSQC spectra. Then 2D NOESY spectra were measured. In total, 2474 NOESY constraints were obtained. Eighty four restraints of the  $\phi$  torsion angle obtained from an HMQC-J experiment were used for structure calculation. After structure calculations in the early stage, the restraints of the  $\chi_1$  torsion angle were added for 16 residues. These residues showed single dominant conformers in early structural calculations, which were consistent with the values of  $J_{\alpha\beta}$ ,  $J_{\alpha\beta}$  obtained from E-COSY experiments. The final 20 structures showed no restraint violations greater than 0.3 Å. The RMSD of the top 20 conformers was 0.37 Å for backbone atoms, and 0.95 Å for heavy atoms respect to the mean structure. Although the major folding was similar to each other for the solution structure of ferrocycytochrome  $c_3$  and the crystal structure of ferricytochrome  $c_3$ , the region involving heme 1 and heme 2 was different. This is consistent with the reported solution structure of *Desulfovibrio vulgaris* Hildenborough ferrocycytochrome  $c_3$ , which is highly homologous with *DvMF* cytochrome  $c_3$ . From the backbone dynamic analysis, the average value of the  $S^2$ , in the reduced state is larger than that in the oxidized state, suggesting that backbone of *DvMF* cytochrome  $c_3$  is slightly more rigid in the reduced state than in the

oxidized state. However, the region involving heme1 and heme2 shows more flexibility in the reduced state than in the oxidized state.

## II-G Application of Optical Vortices to Spectroscopy

### II-G-1 Efficient Generation of Optical Vortices and the Application to Atom Manipulation

**SASADA, Hiroyuki**  
(IMS and Keio Univ.)

Recently optical vortices have attracted considerable attentions because of the phase singularity and the characteristic intensity distribution. In particular, the dark region is very useful to trap and guide cold atoms provided by laser cooling.<sup>1)</sup> Several methods of generating the optical vortices have been reported so far, but their efficiencies are rather low.

We have demonstrated a simple and efficient generation of optical vortices using only glass plates and an astigmatic mode converter. A Gaussian beam successively passes  $N$  edges of thin glass plates, each of which imposes a  $\pi$ -phase difference to a part of the beam transmitting through the glass plate from the other part traveling in the air. The resultant beam has  $N$  nodal lines, and then is further led into a mode converter, which provides  $N$  appreciable optical vortices. The power efficiency is measured to be 72, 64, and 53% for  $N = 1, 2,$  and  $3,$  respectively.

#### Reference

- 1) T. Kuga, Y. Torii, N. Shiokawa, T. Hirano, Y. Shimizu and H. Sasada, *Phys. Rev. Lett.* **78**, 4713 (1997).

## II-H Molecular and Electronic Structures of Metallofullerenes

The continued interest in radical ions of fullerenes and metallofullerenes has resulted from the discovery of superconductivity in the CT complexes of alkali metals with fullerenes. Spectroscopic information concerning the electronic and spin states of the metallofullerenes has been obtained by cw- and pulsed-EPR measurements.

### II-H-1 High-Field/High-Frequency ESR Study of Gd@C<sub>82</sub>

FURUKAWA, Ko; OKUBO, Shingo; KATO, Tatsuhisa; KATO, Haruhito<sup>1</sup>; SHINOHARA, Hisanori<sup>1</sup>  
(<sup>1</sup>Nagoya Univ.)

The X-band ESR investigations of La@C<sub>82</sub>, Y@C<sub>82</sub>, and Sc@C<sub>82</sub> have been reported. In these metallofullerenes, the electronic structures of the metal atoms are described as  $nd^{1(n+1)}s^2$ . They have been reported that these metallofullerenes have the doublet ground states originating in the organic  $\pi$  radical of the C<sub>82</sub> trianion via the electron transfer from metal atoms to C<sub>82</sub> cage. On the other hand, the electronic structure for Gd atom is described as  $4f^75d^16s^2$ , and the ground high-spin state is expected. Our purpose in this work is the examination of the spin state of Gd@C<sub>82</sub> and of the cage effect of the fullerene C<sub>82</sub>. Highly purified Gd@C<sub>82</sub> was obtained by high performance liquid chromatographic (HPLC) method. We examined Gd@C<sub>82</sub> in CS<sub>2</sub> solutions in terms of X- and W-band ESR spectroscopy. Figure 1 shows the X-band ESR spectrum for Gd@C<sub>82</sub> in CS<sub>2</sub> solution at 1.5 K. The spectrum pattern corresponds to that for the high-spin systems with large fine structure. The unsymmetrical spectral feature was given because of the large zero-field splitting parameter  $D$  and  $E$ , and prevented us from an easy spectral simulation. The W-band ESR measurement was performed to simplify the spectrum of Gd@C<sub>82</sub>.

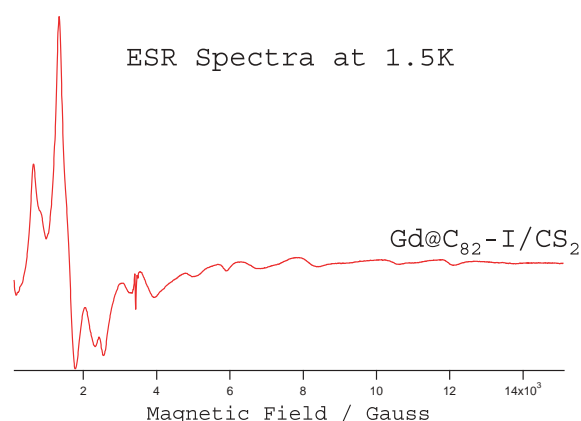


**Figure 1.** The X-band ESR spectrum for Gd@C<sub>82</sub> in CS<sub>2</sub> solution at 1.5 K.

### II-H-2 Spin State of an Inclusion Complex of a Cyclic Dimer of Metalloporphyrin with La@C<sub>82</sub>

TOYAMA, Namiki; KATO, Tatsuhisa; AKASAKA, Takeshi<sup>1</sup>; TASHIRO, Kentaro<sup>2</sup>; AIDA, Takuzo<sup>2</sup>  
(<sup>1</sup>Univ. Tsukuba; <sup>2</sup>Univ. Tokyo)

A paramagnetic metallofullerene is a nice building block for a molecular magnet. Wrapping of a metallofullerene with larger  $\pi$ -conjugated molecular envelopes is of great interest, which may lead to an extension of the super-molecular magnet in a 3D-fashion. Tokyo group of authors has synthesized a cyclic dimer of metalloporphyrin,<sup>1)</sup> as shown in the figure, and reported the big association constant of  $6.7 \times 10^5 \text{ M}^{-1}$  for the inclusion complex of a cyclic dimer of zinc porphyrin with C<sub>60</sub> in benzene solution. The big association properties would come from the flexibility of linkers between two porphyrins. The hexamethylene linkers of the dimer were folded to adjust the porphyrin-porphyrin distance, and the porphyrin macrocycles were slightly distorted from the planar structure so as to fit the shape of C<sub>60</sub>. The electron spin state of an inclusion complex of a cyclic dimer of metalloporphyrin with metallofullerene was investigated by means of pulsed electron spin resonance (ESR) measurement. The direct experimental evidence of the coupled spin state of  $S = 3/2$  was obtained for the cyclic dimer of copper-porphyrin with La@C<sub>82</sub> by the nutation measurement of pulsed ESR. A big variety would be expected for the spin state of the inclusion complex in terms of the combination of metals on a porphyrin and a fullerene.

#### Reference

- 1) K. Tashiro, T. Aida, J.-Y. Zheng, K. Kinbara, K. Saigo, S. Sakamoto and K. Yamaguchi, *J. Am. Chem. Soc.* **121**, 9477 (1999).

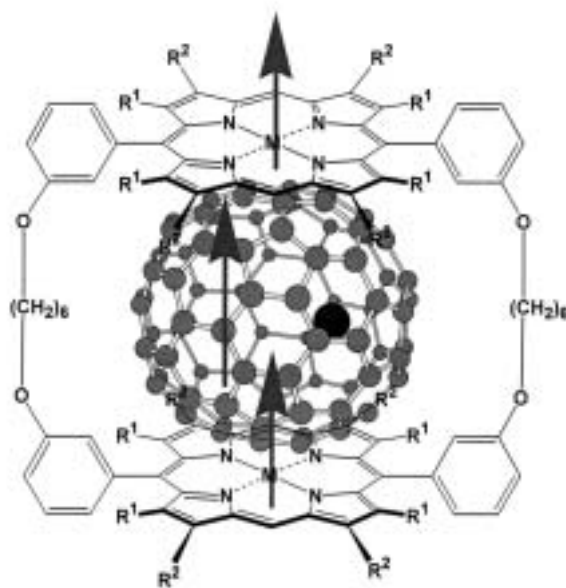


**Figure 1.** Molecular model of an inclusion complex of a cyclic dimer of metalloporphyrin with metallofullerene La@C<sub>82</sub>.

## II-I High Field and Pulsed Electron Spin Resonance Spectroscopy

Electron spin resonance (ESR) spectroscopy has been a powerful technique for the characterization of radical species. The modern development of EPR spectroscopy enables us to investigate the heterogeneous and disordered system in detail. Especially the high frequency and pulsed EPR methods achieve the substantial resolution enhancement of spectrum. The advanced EPR spectroscopy is applied to study on the reaction mechanism in the heterogeneous system and the detection of the dication species.

### II-I-1 Radical Products in Mechanochemical Dechlorination of Hazardous Organochlorine on CaO Surface

KATO, Tatsuhisa; IKOMA, Tadaaki<sup>1</sup>; ZHANG, Qiwu<sup>2</sup>; SAITO, Fumio<sup>2</sup>; AKIYAMA, Kimio<sup>1</sup>; TERO-KUBOTA, Shozo<sup>1</sup>

(<sup>1</sup>Inst. Chem. React. Sci., Tohoku Univ.; <sup>2</sup>Inst. Adv. Mater. Process., Tohoku Univ.)

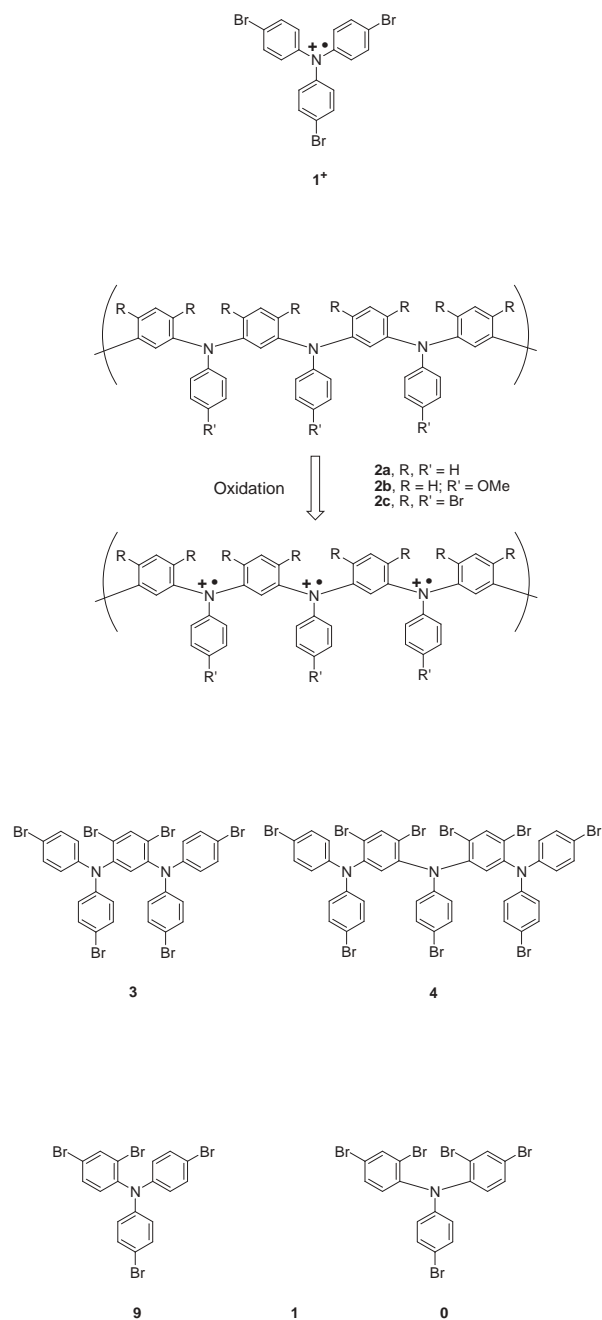
It is widely recognized that hazardous chlorinated organic compounds such as poly-chloro-dibenzoparaoxin (dioxin), poly-chloro-benzofuran and coplanar poly-chloro-biphenyl (PCB) are the most dangerous pollutants to our environment and health. Such great concern has led to many investigations for the complete decomposition of these toxic compounds. Recently mechanochemical method with alkaline earth metals (Mg, Ca) or their oxides have attracted attention as a practically simple and useful process to degrade chlorinated organic compounds. It is, therefore, desired to investigate the reaction mechanism of the mechanochemical dechlorination that is a solid state reaction. The advanced EPR spectroscopy is applied to study the reaction mechanism in the mechanochemical dechlorination of organochlorine using inorganic reactants. For the first time, we detected the paramagnetic products created by grinding 3-chlorobiphenyl (BP-Cl) with calcium oxide (CaO) as reactant in a ball mill, which is one of the promising ways to detoxify hazardous chlorinated organic compounds. Those products were attributed to phenoxy radicals coming from BP-Cl and trapped electrons in oxygen vacancies on the reactant surface by using high frequency and pulsed electron paramagnetic resonance spectroscopies. A radical mechanism for the destruction of organochlorine was proposed, since the good correlation between the dechlorination efficiency and the radical yield were observed. The mechanical stressing may induce the electron transfer from O<sup>2-</sup> site on the surface of CaO to organic compounds and the produced organic anion radicals undergo an effective self-dissociation of the chlorine-carbon bond.

### II-I-2 Facile Synthesis, Crystal Structures, and High-Spin Cationic States of All-*para*-brominated Oligo(*N*-phenyl-*m*-aniline)s

KANEMOTO, Katsuichi; KATO, Tatsuhisa; ITO, Akihiro<sup>1</sup>; INO, Haruhiro<sup>1</sup>; TANAKA, Kazuyoshi<sup>1</sup>

(<sup>1</sup>Kyoto Univ.)

Syntheses of both the dimer (**3**) and the trimer (**4**) of all-*para*-brominated poly(*N*-phenyl-*m*-aniline)s (**2c**) were achieved in a one-pot procedure from the parent non-brominated oligomers and benzyltrimethylammonium tribromide (BTMA-Br<sub>3</sub>), see Scheme 1. An X-ray crystallographic analysis revealed that **4** has a U-shaped structure, suggesting that **2c** easily adopts helical structures. Furthermore, the redox properties were investigated by the UV-vis and EPR measurements. It was confirmed that the both **3** and **4** can be oxidized into the dications **3**<sup>2+</sup> and **4**<sup>2+</sup> with triplet spin-multiplicity. In order to identify the spin multiplicity of this species, we adopted the pulsed EPR method based on the fact that the magnetic moments with distinct spin quantum numbers (*S*) precess with their specific nutation frequency ( $\omega_n$ ) in the presence of a microwave irradiation field (*B*<sub>1</sub>) and a static magnetic field (*B*<sub>0</sub>). Figure 1 shows the relation between the EPR spectra observed at 5 K and its transient nutation spectra in a 2-D contour representation. Namely, the projection on the magnetic field axis corresponds to the usual EPR spectrum, while the projection on the frequency axis to the nutation spectrum. The intense peak observed at 3410 G (3415 G) is expected to be  $|1/2, +1/2\rangle \leftrightarrow |1/2, -1/2\rangle$  transition of the doublet species **3**<sup>+</sup> (**4**<sup>+</sup>) and had the nutation frequency of 30.0 MHz (30.0 MHz), indicating  $\omega_1 = 30$  MHz. On the other hand, two peaks at 3325 and 3510 G (3395 and 3445 G) had the same nutation frequency of 43.8 MHz (43.9 MHz), suggesting the presence of a high-spin cationic species of **3** (**4**). Here, the frequency ratio ( $\omega_n/\omega_1$ ) of 43.8/30.0 (43.9/30.0) is in good agreement with the ratio of  $\sqrt{2}$  expected for  $|1, 0\rangle \leftrightarrow |1, \pm 1\rangle$  transition of the triplet state. As a result, the high-spin species generated by excess of SbCl<sub>5</sub> can be regarded as **3**<sup>2+</sup> (**4**<sup>2+</sup>).



Scheme 1. Molecular structures of aromatic amines.

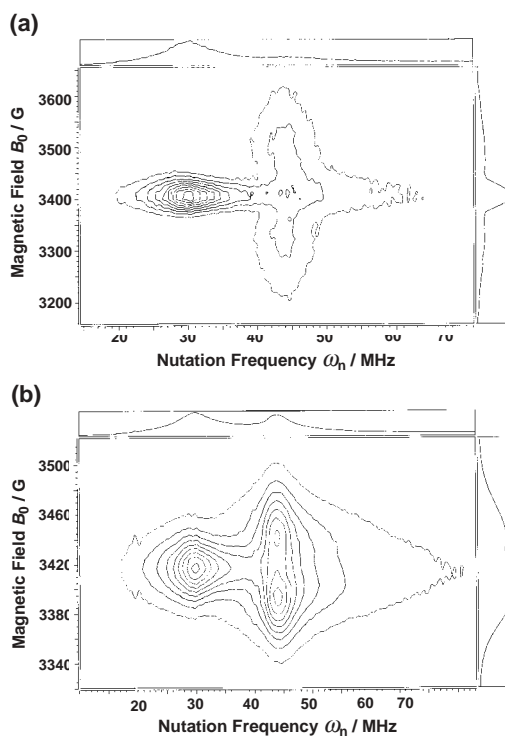


**Figure 1.** Field-swept electron spin nutation spectra of (a) **3** and (b) **4** oxidized by excess  $SbCl_5$  in  $CH_2Cl_2$  at 5 K.  $\omega_1$  corresponds to 30 MHz.

## II-J State Correlated Raman Spectroscopy

The vibrational Raman polarizability tensor responds to molecular reorientational relaxation process, and the structural environment in condensed media. The measurement of Raman scattering is a powerful technique for the study of molecular motion and of the mechanism of phase transition. We've built up the system of multichannel type detection of Raman scattering combined with the temperature controlled cell.

## II-J-1 Probable Langevin-Like Director Reorientation in an Interface-Induced Disordered $SmC^*$ -Like State of Liquid Crystals Characterized by Frustration between Ferro- and Antiferroelectricity

HAYASHI, Naoki; KATO, Tatsuhisa; AOKI, Takayuki<sup>1</sup>; ANDO, Tomohiro<sup>1</sup>; FUKUDA, Atsuo<sup>1</sup>; SEOMUN, San-Seong<sup>2</sup>  
(<sup>1</sup>Shinshu Univ.; <sup>2</sup>Univ. Dublin)

[*Phys. Rev. Lett.* **87**, 015701 (2001)]

To clarify the thresholdless, hysteresis free V-shaped switching due to frustration between ferro- and antiferroelectricity, we have studied a prototype binary mixture system. The apparent orientational order parameters,  $\langle P_2 \rangle$  and  $\langle P_4 \rangle$ , obtained from polarized Raman scattering in thin homogeneous cells indicate that substrate interfaces induce some randomization of local in-plane directors at the tip of the V. Their correlation length,  $\xi_{\parallel} \approx 3.5$  nm and  $\xi_{\perp} \approx 75$  nm, have been estimated by assuming the Langevin-like reorientation. Because of the much shorter  $\xi_{\parallel}$  and  $\xi_{\perp}$  than the visible light wavelength, the switching process looks uniform.

## II-J-2 Orientational Distributions in Smectic Liquid Crystals Showing V-Shaped Switching Investigated by Polarized Raman Scattering

HAYASHI, Naoki; KATO, Tatsuhisa; AOKI, Takayuki<sup>1</sup>; ANDO, Tomohiro<sup>1</sup>; FUKUDA, Atsuo<sup>1</sup>; SEOMUN, San-Seong<sup>2</sup>  
(<sup>1</sup>Shinshu Univ.; <sup>2</sup>Univ. Dublin)

The polarized Raman scattering of two types of liquid crystals showing the thresholdless, hysteresis-free V-shaped electro-optic response in thin homogeneous cells was measured in the temperature range of antiferroelectric smectic phase. One sample was one component of Inui mixture [compound **a** in the Figure 1(A)] and the other was so-called Mitsui mixture [Figure 1(B)]. The apparent orientational order parameters,  $\langle P_2 \rangle$  and  $\langle P_4 \rangle$  were evaluated for the C–C stretching mode of phenyl ring. The obtained order parameters at the tip of the V-shaped switching were  $\langle P_2 \rangle = 0.70$  and  $\langle P_4 \rangle = 0.35$  for the compound **a**,  $\langle P_2 \rangle = 0.59$  and  $\langle P_4 \rangle = 0.20$  for the Mitsui mixture. The model calculations confirmed two extreme distribution of the local in-plane director at the tip of the V. The compound **a** exhibited a small distribution, while the Mitsui mixture did a very large distribution. The difference in the distribution of two types of liquid crystals at the tip of the V was explained by the barrier between synclinal and anticlinal ordering in adjacent layers. The small barrier gave a large distribution at the tip of the V in the dynamic switching, consequently triggered the V-shaped switching even in the first run. On the other hand, the large barrier did a small distribution and the tristable switching.

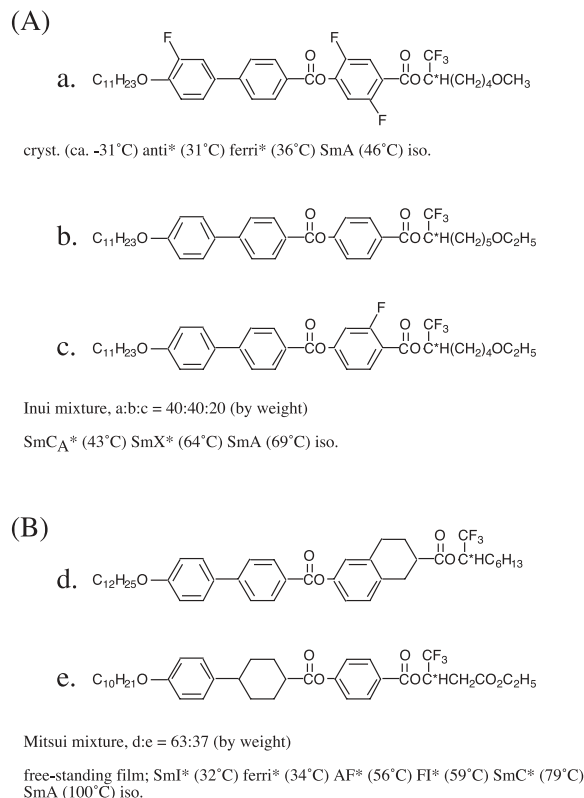


Figure 1. The Inui mixture (A) and the Mitsui mixture (B).